

Geometric and Physical Reduced Order Modeling Applied to CFD results

Alexandre M S Costa (amscosta@uem.br)

Departamento de Engenharia Mecânica, Universidade Estadual de Maringá, Av Colombo 5790, Maringá, PR, Brazil

Marcelo J Alba

Departamento de Física, Universidade Tecnológica Federal do Paraná, R Marcilio Dias 635, Apucarana, PR, Brazil

Marco E Biancolini

Department of Enterprise Engineering “Mario Lucertini”, University of Rome “Tor Vergata”, Rome, Italy

Highlights

- Using Reduced Order Models derived from CFD simulations can be computationally fast and inexpensive
- Geometric Reduced Order Models incorporating spatial input parameters can enhance the applicability of the method
- Geometric Reduced Order Models coupled with physical Reduced Order Models is a relatively recent development

Abstract

Reduced Order Models (ROM) derived from CFD simulations has been reported in recent years. They can include physical and/or spatial parameter variation in their predictions. The integration of spatial parameter variation (geometric ROM) is a relatively new approach, and it is exemplified in this short note.

Introduction

During the last decades, Reduced Order Models (ROM) has been applied for engineering problems tackled by Computational Fluid Dynamics (CFD) (Lang *et al.*, 2009; Jung *et al.*, 2011; Ballarin, *et al.*, 2015; Ballarin *et al.*, 2016; Han *et al.*, 2020; Biancolini, *et al.*, 2020; Zhong *et al.*, 2020; Calka *et al.*, 2021). ROM evolves from the division of a higher order problem (Chinesta *et al.*, 2014) into two tasks: one, computationally expensive (comprising the ROM object generation), and other, computationally cheaper, related to the ROM object consumption. The consumption task can be done in a lighter hardware platform, linked to a multiscale model of an industrial plant, or digital twin (Laubenbacher, *et al.* 2021; Sancarlos, *et al.* 2021; Singh, *et al.*, 2021).

The accessibility of the whole solutions fields, e.g., velocities, from the ROM object, place them apart from response surface methods applied to CFD solutions (Myers, *et al.*, 2016) since the latter can be summarized by obtaining correlations between a set of

input and output parameters, e.g., pressure drop (output parameter) and inlet velocity (input parameter). A brief mathematical detailing of the ROM technique is present in the appendix.

In general terms, the ROM object generation starts from the learning of the physics of a given model (Maquart et al., 2020). Referring to Figure 1, the *LEARNING SUBSET* is chosen from the whole field of solutions available from the *CFD SIMULATION DATA SET*. Each element of the *CFD SIMULATION DATA SET* corresponds to the solution for a list of input parameters values (design point). The generation of the list of input parameters employs techniques from the Design of Experiments (Montgomery, 2013; Almeida et al., 2020). For each design point, the CFDs solution field for each variable is stored in a so called snapshot file. The remaining subset of snapshots (*VALIDATION SUBSET* in Figure 1) is used in numerical verification (*ROM ACCURACY CHECK*).

For the physical ROM, the input parameters consists of fluid properties or boundary condition values. Additionally, for geometric ROM, the input parameters consists of geometric spatial values. An important requirement for the geometric ROM construction, is mesh generation for the modified geometric values must be isotopological, i.e., keeps the same number of nodes. This mesh's feature make compression techniques readily applicable.

In this short note is detailed the steps depicted in Figure 1, for the generation of geometric ROM and its posterior use combined with a physical ROM. The schematized steps were recently implemented using the CFD solver ANSYS FLUENT 2021R1 and Twin Builder 2021R1. For isotopological mesh generations, related to the geometric ROM construction, were employed the RBF Morph for Fluent v. 2.12 package. A primer on package's numerics can be found in Biancolini (2017).

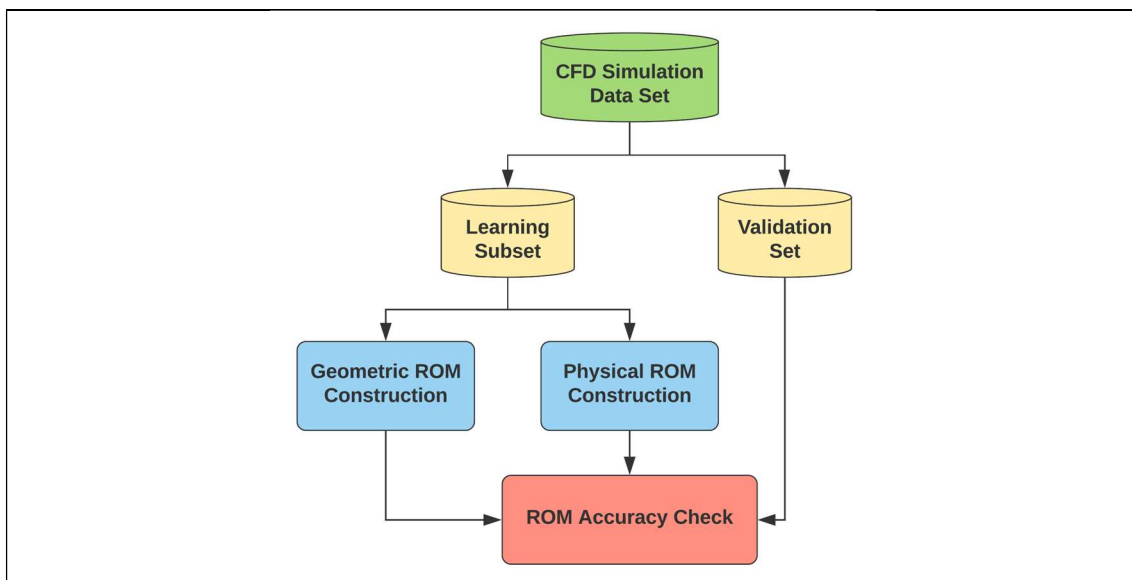


Figure 1 – ROM from CFD simulations

Methodology

Figure2(a) illustrates the geometry and coordinate system used as a starting point for CFD simulations. It represents an existing lab-scale stirred tank mixer with inclined

blades(Moro,2016). To simulate the rotating domain, the moving reference frame (MRF) approach was used. The polyhedrals generated in the ANSYS Meshing 2021R1 software was constituted by 251,897 cells .Figure 2(b) presents a section detail of the mesh. As this refinement level was demonstrated adequate (Moro, 2016), no further mesh refinement was done.

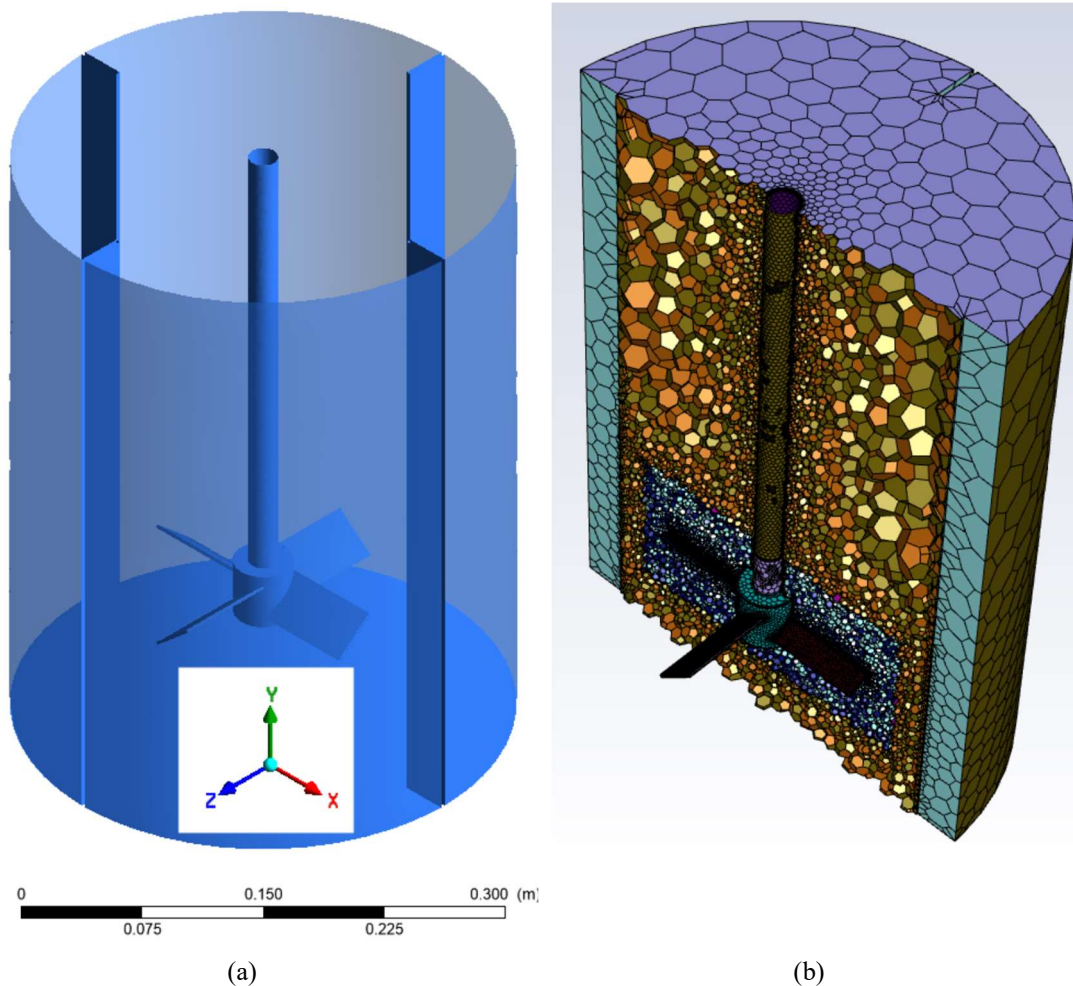


Figure 2 (a) Mixer geometry and (b) detail of polyhedral mesh for half domain

The standard $k-\omega$ turbulence model was adopted. The CFD solver used was pressure-based and with coupled equations (PBCS), available in ANSYS Fluent 2021R1 software. The pseudo-transient approach was also adopted with explicit relaxation factors of 1, 1, 0.75, 0.5, 0.5 (density, turbulent kinetic energy, specific turbulent kinetic energy dissipation, momentum, pressure). The spatial discretization scheme was second-order upwind for pressure, momentum, turbulent kinetic energy, and specific dissipation of turbulent kinetic energy.

For the construction of the ROM, 100 CFD simulations were generated. For such simulations, the physical input parameters depicted in Table 1 could vary in the following ranges: fluid density ρ (1000-1400 kg/m³); viscosity μ (10⁻³-10⁻² kg/(m.s)); blade rotation speed ϕ (40-400 rad/s). Accordingly, it is emphasized that permitted ranges of variation of parameters followed the actual limits of rotation (Moro, 2016); and the density and viscosity to aqueous solutions (Melinder, 2010). Furthermore, the geometric input parameter, the blade diameter D could vary in the range 0.160-0.175 [m]. The diameter change was attained by using the RBF Morph software for Fluent.

Table 1. Summary of Simulation Points for ROM generation.

Design Point #	ρ (kg m ⁻³)	μ (kg m ⁻¹ s ⁻¹)	ϕ (rad/s)	D (m)	Design Point #	ρ (kg m ⁻³)	μ (kg m ⁻¹ s ⁻¹)	ϕ (rad/s)	D (m)
1	1325.889	0.00246	271.9545	0.160894	51	1110.41	0.004755	386.7119	0.164522
2	1362.317	0.008149	176.2994	0.17023	52	1271.881	0.001447	236.8501	0.170516
3	1050.795	0.003801	332.169	0.160635	53	1262.039	0.009124	227.6089	0.169995
4	1365.35	0.005757	231.8172	0.161072	54	1065.045	0.009503	123.374	0.168087
5	1252.944	0.002491	166.2618	0.167825	55	1047.599	0.005418	216.0032	0.170472
6	1039.016	0.006418	378.0406	0.161451	56	1199.346	0.005403	264.6616	0.169998
7	1111.399	0.003367	355.3394	0.172272	57	1383.898	0.004039	284.4888	0.162672
8	1218.753	0.006887	238.0563	0.172263	58	1136.154	0.0091	182.3855	0.16192
9	1383.003	0.007203	264.091	0.170837	59	1234.107	0.004323	172.2772	0.174986
10	1385.955	0.007733	251.3361	0.162248	60	1089.525	0.002001	395.6735	0.162567
11	1063.045	0.005055	114.7872	0.169894	61	1300.507	0.008022	53.58599	0.160489
12	1388.237	0.001754	148.4487	0.167779	62	1102.038	0.004508	358.6605	0.168418
13	1382.867	0.003061	209.5324	0.174595	63	1202.383	0.003175	368.7833	0.173228
14	1194.15	0.00922	122.9757	0.169735	64	1279.631	0.004635	326.6262	0.170038
15	1320.112	0.002371	343.9512	0.172005	65	1356.361	0.001868	75.53642	0.162856
16	1056.755	0.008432	110.1151	0.166807	66	1383.717	0.002188	134.2736	0.165534
17	1168.705	0.005845	121.3318	0.166486	67	1218.886	0.009478	160.7285	0.166911
18	1366.294	0.009965	101.4549	0.17238	68	1055.45	0.009605	284.7021	0.174725
19	1316.883	0.001704	121.9591	0.161252	69	1059.718	0.006177	89.15913	0.162346
20	1383.797	0.004984	196.8515	0.161998	70	1103.003	0.001538	299.6419	0.172833
21	1262.296	0.00196	151.9968	0.162601	71	1336.287	0.003113	78.43427	0.169671
22	1014.285	0.009657	372.4167	0.165864	72	1101.713	0.004178	275.3526	0.165644
23	1339.652	0.001042	194.8747	0.172471	73	1325.714	0.008391	217.9026	0.162864
24	1373.597	0.007974	106.5339	0.17205	74	1097.41	0.001139	320.4586	0.166424
25	1271.494	0.008356	365.7571	0.160907	75	1371.705	0.001387	297.4133	0.16723
26	1303.096	0.008818	392.7094	0.165989	76	1139.994	0.002521	365.3394	0.161809
27	1297.253	0.00176	197.9932	0.167903	77	1078.638	0.006842	360.7321	0.168843
28	1156.891	0.004598	80.00292	0.166252	78	1100.434	0.007586	160.2987	0.163393
29	1262.191	0.003339	132.9033	0.169853	79	1246.418	0.00683	291.5485	0.165769
30	1068.475	0.008201	187.1391	0.16942	80	1189.316	0.005058	111.2115	0.168745
31	1282.418	0.004883	254.1626	0.16438	81	1140.664	0.005923	50.99474	0.163777
32	1012.733	0.009196	134.3962	0.166475	82	1332.331	0.003667	307.8667	0.164357
33	1110.769	0.002637	257.0235	0.160232	83	1234.106	0.007702	220.0081	0.169256
34	1018.469	0.003374	296.0377	0.174761	84	1219.889	0.002701	212.772	0.163979
35	1038.853	0.00231	119.8288	0.162508	85	1366.877	0.007181	365.7	0.172366
36	1329.383	0.002225	82.27035	0.161593	86	1114.336	0.002652	259.552	0.17474
37	1277.931	0.008824	146.8033	0.165586	87	1302.88	0.004316	262.3599	0.170954
38	1126.84	0.006217	154.7602	0.162972	88	1301.492	0.006631	349.3992	0.165158
39	1380.089	0.005949	192.7	0.167345	89	1152.178	0.008022	329.9762	0.168761
40	1013.778	0.002305	222.829	0.165092	90	1227.129	0.00173	247.6197	0.161617
41	1175.498	0.008677	70.78569	0.174274	91	1030.342	0.009364	105.8521	0.173595
42	1152.623	0.006598	134.4936	0.173805	92	1021.58	0.007981	126.3755	0.173195
43	1306.207	0.004159	328.3653	0.16079	93	1212.319	0.005381	359.1443	0.172266
44	1318.08	0.005619	50.5193	0.171068	94	1311.667	0.004923	50.32269	0.163911
45	1074.749	0.004616	374.3875	0.164037	95	1373.604	0.005021	216.3645	0.168915
46	1195.906	0.001684	302.9191	0.166343	96	1051.962	0.003757	100.4538	0.160338
47	1178.234	0.003159	215.8992	0.168218	97	1227.529	0.005577	392.325	0.166379
48	1258.525	0.00211	248.269	0.174141	98	1187.756	0.005597	296.57	0.164691
49	1283.746	0.002655	125.4221	0.166266	99	1004.761	0.008359	220.1698	0.162422
50	1301.875	0.00316	205.1856	0.174746	100	1134.849	0.008153	209.5918	0.162681

The use of ROM Builder Preprocessing extension inside the ANSYS Fluent standalone solver, allowed to automate the running of the multiple CFD simulations in Table 1. A Scheme language script was used to program the RBF Morph callings during these snapshots generations. Subsequently, geometric and physical ROM generation is performed inside the Static ROM Builder called inside the Twin Builder – Electronics Desktop 2021R1.

In the next section some key aspects related to the ROM objects will be discussed.

RESULTS AND DISCUSSION

The ROM objects were produced and analysed for the solutions fields: Velocity, Velocity Magnitude, Turbulent Kinetic Energy, Specific Dissipation Rate and Wall Shear Stress. In the appendix/supplement is presented a series of short videos showing the effect of the input parameters in the solution fields from the ROM objects.

Following the mathematical definitions of Appendix A, an error analysis was performed next. The error analysis was planned from Figure 3, relating the number of learning snapshots (50, 75 and 100) and the number of modes.

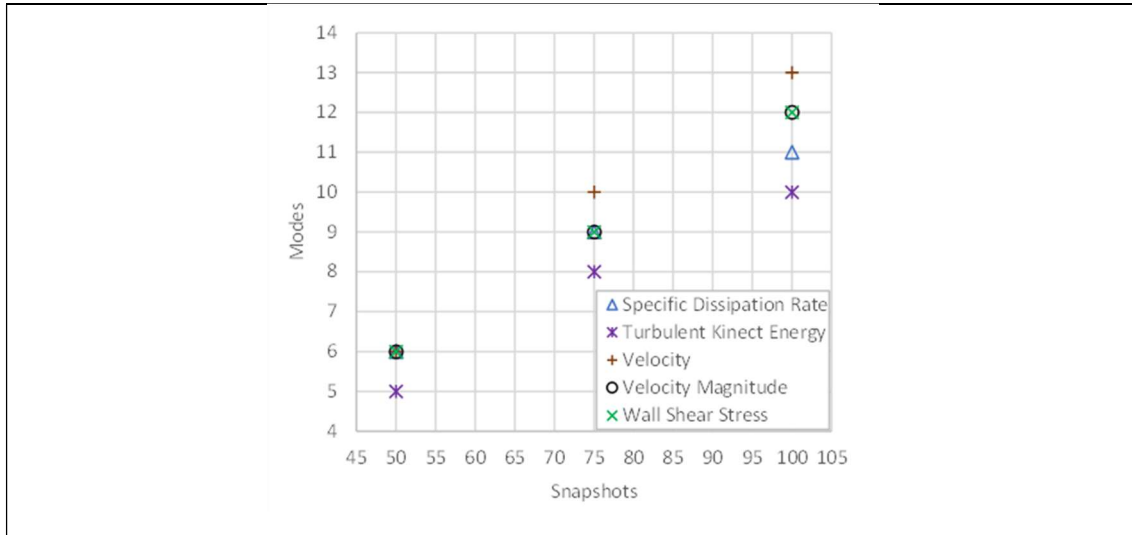


Figure 3 - Combination between number of snapshots and number of modes for the simulated fields

It was noticeable that the increase in the number of modes and the number of learning snapshots has a direct impact on the computational cost. However, for the considered problem, this extra computational cost did not make the procedure unfeasible.

Figure 4 presents the errors as a function of the number of modes considered in the construction of the ROM. For all the solution fields, there is a tendency to decrease the error with the increase in the number of modes considered. With the exception of the specific dissipation rate for the case of 100 snapshots, where both errors have the same value, it is also possible to verify that the ROM Relative Error (Eq. 03, from the appendix) is always greater than the Reduction Relative Error (Eq. 04, from the appendix). The ROM Relative Error is generated after the construction of the ROM, while the Reduction Relative Error is generated right after choosing the number of modes to be considered for the ROM construction, that is, the Reduction Relative Error is calculated before the ROM Relative Error.

The increase in the number of modes implies in decrease of errors shown in Figure 5. The behavior is valid for all solution fields. Despite a more significant decrease in errors for the Reduction Relative Error, ranging between 44% and 58% (14 percentage points), the ROM Relative Error has a more accentuated rate of change, ranging between 25% and 48% (23 percentage points) depending on the chosen number of modes.

Therefore, the use of a greater number of learning snapshots and modes is justified, even with the increase in computational cost, especially when the error obtained is greater than expected. For this study, a target error below 7% was chosen, a value that was reached for all solutions fields (smaller values of the green lines in figure 4).

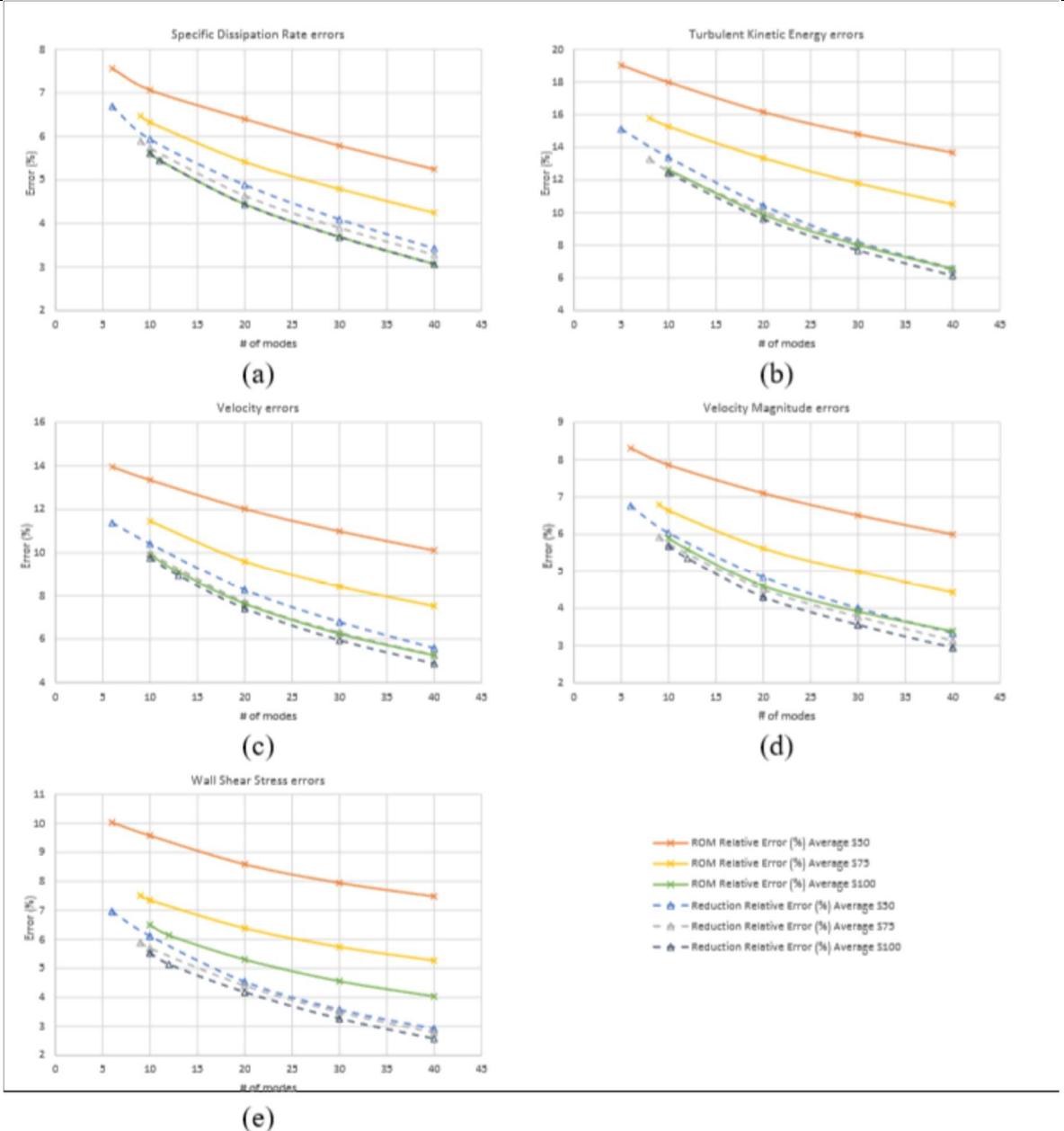


Figure 4. ROM Relative Errors and Reduction Relative Errors versus number of modes for 50, 75 and 100 learning 100 snapshots, in the (a) SDR, (b) TKE, (c) VEL, (d) VEL_MAG and (e) WSS.

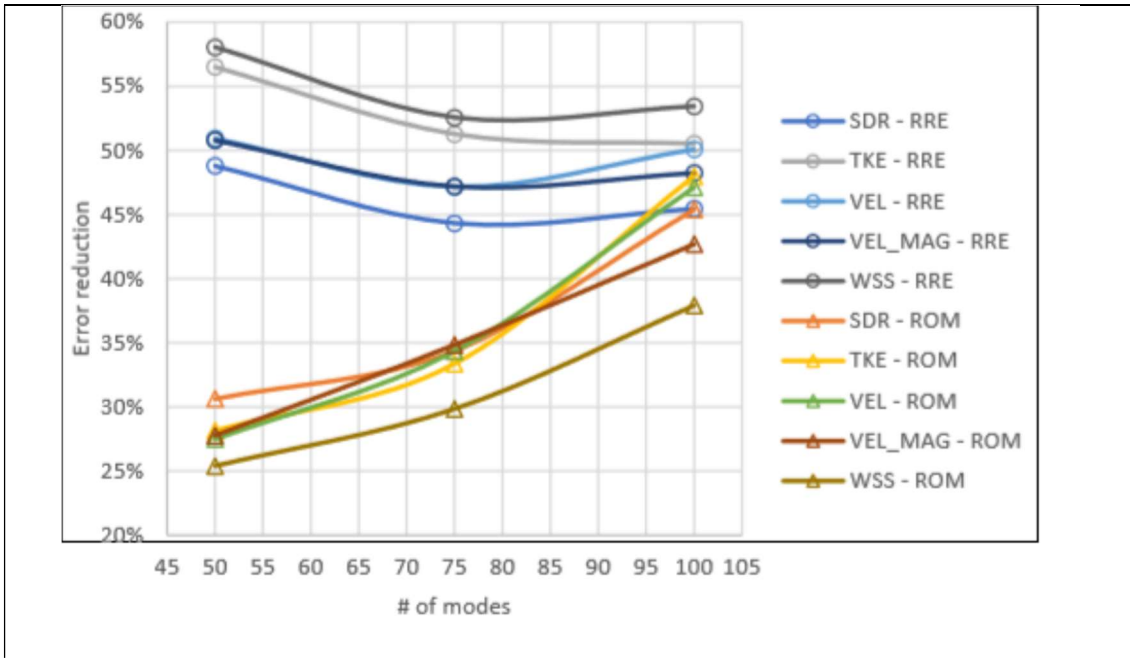


Figure 5. Error decrease versus number of modes considered in solutions fields for Reduction Relative Error (RRE) and ROM Relative Error (ROM).

CONCLUSIONS

In this short note the steps for geometric and physical ROM object generation from CFD simulations were presented. Recent development incorporating spatial parameter variation for geometric ROM objects adds extra flexibility to the range of engineering applications that can benefit from the ROM technique. The errors associated to the use of results from the ROM object instead the full CFD simulations were due to the number of the learning snapshots and the number of modes. For each variable field, those numbers can be selected by the user for reaching a given target error. Conversely to the CFD simulations, all the tasks involved in the ROM object generation are computationally fast. At last, the ROM object consumption requires a lighter hardware platform than the CFD simulations.

SUPPLEMENT

Videos available DOI: [10.5281/zenodo.7075312](https://doi.org/10.5281/zenodo.7075312)

REFERENCES

- Acar, E., 2010, Various approaches for constructing an ensemble of metamodels using local measures. *Structural and Multidisciplinary Optimization*, Vol. 42, n. 6, pp. 879-886.
- Almeida, P., and Costa, A.M.S., Souza, M., 2020. Direct and Indirect Optimization of CFD Experiments in Microfluidics: A Study of Case. In: *ENCIT 2020 - 18th Brazilian Congress of Thermal Sciences and Engineering*.
- Ballarin, F., 2015. Reduced-order models for patient-specific haemodynamics of coronary artery bypass grafts. PhD thesis, Department of Mathematics, Politecnico di Milano.
- Ballarin, F., Faggiano, E., Ippolito, S., Manzoni, A., Quarteroni, A., Rozza, G., and Scrofani, R. 2016. Fast simulations of patient-specific hemodynamics of coronary artery bypass grafts based on a POD –

- Galerkin method and a vascular shape parametrization. *Journal of Computational Physics*, Vol. 315, pp. 609–628.
- Ben Salem, M., and Tomaso, L., 2018. Automatic selection for general surrogate models”. *Structural and Multidisciplinary Optimization*, Vol. 58, n. 2, pp. 719-734.
- Biancolini, M. E., 2017. *Fast Radial Basis Functions for Engineering Applications*. Springer International Publishing.
- Biancolini, M.E., Capellini, K., Costa, E., Groth, C., and Celi, S.X., 2020. Fast interactive CFD evaluation of hemodynamics assisted by RBF mesh morphing and reduced order models: the case of aTTA modeling. *International Journal on Interactive Design and Manufacturing*, Vol. 14, pp. 1227-1238.
- Calka, M., Perrier, P., Ohayon, J., Grivot-Boichon, C., Rochette, M., Payan, Y., Machine-Learning based model order reduction of a biomechanical model of a tongue. 2021. *Computational Methods and Programs in Biomedicine*, Vol. 198, 105786.
- Carlberg, K., Farhat, C., Cortial, J., and Amsallem, D., 2013. The GNAT Method for Nonlinear Model Reduction: Effective Implementation and Application to Computational Fluid Dynamics and Turbulent Flows. *Journal of Computational Physics*, Vol. 242, pp. 623-647.
- Chinesta, F., Keunings, R., and Leygue, A., 2014. *The Proper Generalized Decomposition for Advanced Numerical Simulations*. Springer International Publishing.
- Driscoll, T. A., Braun, R. J., 2018. *Fundamentals of Numerical Computation*. Society for Industrial and Applied Mathematics. pp. 293-310
- Han, S., Schirmer, C.M., Modarres-Sadeghi, Y., 2020. A reduced-order model of a patient-specific cerebral aneurysm for rapid evaluation and treatment planning. *Journal of Biomechanics*, Vol. 103, 109653.
- Jung, S.K., Shin, S., Myong, R.S., Cho, T.H., 2011. An efficient CFD-based method for aircraft icing simulation using a reduced-order model. *Journal of Mechanical Science and Technology*, Vol. 25, n. 3, pp. 703-711.
- Lang, Y., Malacina, A., Bieler, L.T., Munteanu, S., Madsen, J.I., and Zitney, S.E., 2009. Reduced Order Model Based on Principal Component Analysis for Process Simulation and Optimization. *Energy & Fuels*, Vol. 23, pp. 1695-1706.
- Laubenbacher, R., Sluka, J.P., Glazier, J.A., 2021. Using digital twins in viral infection. *Science*, Vol. 371, 6534, pp. 1105-1106.
- Maquart, T., Wenfeng, Y., Elguedj, T., Gravouil, A., Rochette, M., 2020. 3D volumetric isotopological meshing for finite element and isogeometric based reduced order modeling. *Computer Methods in Applied Mechanics and Engineering*, Vol. 362, 112809.
- Melinder, A., 2010. *Properties of Secondary Working Fluids for Indirect Systems*. International Institute of Refrigeration.
- Montgomery, D.C., 2013. *Design and Analysis of Experiments*, Wiley.
- Moro, F.R., 2016. Estudo para a otimização de um impelidor de pás inclinadas em um tanque agitado através da Fluidodinâmica Computacional (CFD) (in Portuguese). Master’s Thesis, Graduate Program in Mechanical Engineering, Universidade Estadual de Maringá, Maringá, Brazil.
- Myers, R.H., Montgomery, D.C., and Cook, and C.M., 2016. *Response Surface Methodology: Process and Product Optimization Using Design of Experiments*, Wiley.
- Sancarlos, A., Cameron, M., Abel, A., From ROM of Electrochemistry to AI-Based Battery Digital and Hybrid Twin. 2021. *Arch Computational Methods Eng*, Vol. 28, pp. 979-105.
- Singh, S., Weeber, M., Birke, K.P., Implementation of Battery Digital Twin: Approach, Functionalities and Benefits. 2021. *Batteries*, Vol. 7, 78.
- Zhong, H., Xiong, Q., Yin, L., Zhang, J., Zhu, Y., Liang, S., Niu, B., and Zhang, X., 2020. CFD-based reduced-order modelling of fluidized-bed biomass fast pyrolysis using artificial neural network. *Renewable Energy*, Vol. 152, pp. 613-626.

Appendix. Reduced Order Model Fundamentals

The ROM construction method derives from the singular value decomposition technique (c.f. Driscoll and Braun, 2018 ;Carlberg *et al.*, 2013) of variable’s fields obtained from CFD solutions. Initially, a vector basis for the solution field of variable X is built. Such base is dependent on the selected input parameters. The building follows Eq. (1).

$$M = U\bar{\Sigma}V^* \quad (1)$$

In the previous equation, M is a rectangular matrix whose columns, each corresponding to a snapshot, are composed of the solution fields of the variable X for several values of the input parameters. The $\bar{\Sigma}$ is a diagonal matrix, whose elements $\sigma_0, \dots, \sigma_n$ are called singular values. In Eq. (1) U and V are unitary matrices, where the columns of U and V are composed respectively of the

left singular vectors U_i and the right singular vectors V_i of the matrix M . Also, it must be noticed that the columns of U , termed as modes, represents a basis for the columns of M , and the product UV^* can be viewed as mode coefficients. V^* denotes the complex conjugate of V .

In the next step, the solution field of the variable X is approximated as \hat{X} , a linear combination of r vectors U_i , by means of Eq. (2).

$$\hat{X} = \sum_{i=1}^r \alpha_i U_i \quad (2)$$

The α_i interpolation coefficients are approximated by the genetic aggregation meta-model (Viana *et al.*, 2009; Acar, 2010; Ben Salem and Tomaso, 2018).

To evaluate the accuracy of ROM approximation two relative errors can be defined: The ROM error ε_{total} and the reduction error $\varepsilon_{reduction}$, given by:

$$\varepsilon_{total} = \frac{\|X - \hat{X}\|}{\|X\|} \quad (3)$$

$$\varepsilon_{reduction} = \frac{\|X - X_r\|}{\|X\|} \quad (4)$$

In Eq(4), each column of X_r corresponds to the vector of values of the projection of the i -th snapshot onto the subspace based on the chosen r first modes of the SVD. Can be decreased by increasing the number of modes considered and/or increasing the learning dataset (c.f. Fig. 1)

When the ROM Reduction Error is subtracted from the ROM error the interpolation error is acquired. This error is related to the uncertainty in determination of the mode coefficients α_i . It can decreased by increasing the learning data set.